POLITECNICO DI TORINO
Repository ISTITUZIONALE

Dynamic depreciation for parts produced using laser-based powder bed fusion of polymers

Original
Dynamic depreciation for parts produced using laser-based powder bed fusion of polymers / Calignano, F., Marchiandi, G., Iuliano, L.. - In: THE INTERNATIONAL JOURNAL OF ADVANCED MANUFACTURING TECHNOLOGY. - ISSN 1433-3015. - (2026). [10.1007/s00170-026-17699-1]

Availability:
This version is available at: 11583/3008068 since: 2026-03-02T09:45:07Z

Publisher:
Springer Nature

Published
DOI:10.1007/s00170-026-17699-1

Terms of use:

This article is made available under terms and conditions as specified in the corresponding bibliographic description in the repository

Publisher copyright

(Article begins on next page)

27 November 2026

The International Journal of Advanced Manufacturing Technology
https://doi.org/10.1007/s00170-026-17699-1

ORIGINAL ARTICLE

Dynamic depreciation for parts produced using laser-based powder bed fusion of polymers

Flaviana Calignano[1,2] · **Giovanni Marchiandi**[1,2] · **Luca Iuliano**[1,2]

Received: 18 June 2025 / Accepted: 8 February 2026
© The Author(s) 2026

Abstract

Laser-based powder bed fusion of polymers (PBF-LB/P) is one of the most widely used additive manufacturing technologies for producing complex and customized components. One of the key aspects of this process is the recycling of the powder, which is central to the technology's overall efficiency. During reuse cycles, the powder undergoes inevitable chemical, physical and mechanical changes that directly affect the quality of the final artifacts. This directly impacts process sustainability and production costs. The Sum-of-the-Year's Digits (SOYD) depreciation model, which has been proposed in the literature for metal powders, assumes an initial moderate decline in value, followed by a slower decline upon reuse. However, polymer powders can degrade more quickly than metal powders, reaching a point of no return sooner. Therefore, the SOYD model has been modified by introducing a nonlinear function to better reflect the non-constant loss of value of the powder. Initially, the loss of value accelerates, then stabilizes, and accelerates again towards the end of the powder's useful life. The proposed depreciation model was used in a case study with two scenarios, which considered the varying residual economic values of recycled polyamide 12 (PA12) powder. The analysis shows that the method used to calculate powder reuse, whether in processing cycles or hours, can significantly impact on the overall material cost and, consequently, the final product cost.

Keywords Selective laser sintering · Powder recycling · Cost model · Polyamide 12 · Powder degradation

Abbreviations

α_{loss}	Percentage of the material lost
AM	Additive manufacturing
AR	Aspect ratio
α_u	Acceleration coefficient of degradation
b	Depreciation rate
C_{AM}	Direct hourly cost of the AM system
$C_{buid-Machine}$	Machine costs
$C_{build-Material}$ (p_i)	Cost per part
$C_{m,u}$	Cost of the powder feedstock used in u build cycles
$C_{m,v}$	Cost of the virgin powder
C_{op}	Operator's hourly rate
DDB	Double Declining Balance
e^{-bu}	Decreasing exponential function
M_F	Amount of powder loaded into the feed
M_i	Mass of a part with ith geometry
Ni	Quantity of parts with ith geometry
P_i	Property values of the ith geometry
PA12	Polyamide 12
PA2200	Trade name of EOS GmbH for PA12
PBF-LB	Laser-based powder bed fusion
PBF-LB/M	Laser-based powder bed fusion of metal
PBF-LB/P	Laser-based powder bed fusion of polymer
PDCA	Plan-Do-Check-Act
S	Salvage value or residual value
SOYD	Sum-of-the-Year's Digits
SLN	Straight-Line
T_B	Bed temperature
T_{build}	Total time of build
T_E	Extraction temperature

✉ Flaviana Calignano
flaviana.calignano@polito.it

[1] Department of Management and Production Engineering (DIGEP), Politecnico di Torino, Corso Duca Degli Abruzzi, 24, Turin 10129, Italy

[2] Integrated Additive Manufacturing Center (IAM@PoliTo), Politecnico di Torino, Corso Duca Degli Abruzzi, 24, Turin 10129, Italy

Published online: 19 February 2026

T_{exp}	Laser exposure time
T_m	Melting temperature
T_{recoat}	Recoating time
T_S	Starting temperature
T_{setup}	Time for setting up the machine
$u_{critical}$	Critical point
U_{max}	Maximum number of build cycles or hours
UTS	Ultimate tensile strength
$V_{tot,i}$	Total volume of the part

1 Introduction

Additive manufacturing (AM) has the potential to transform the supply chain radically, redefining stakeholders roles and introducing new business models by enabling more flexible, localized production close to end consumers [1]. To maintain competitiveness in a changing environment, entrepreneurs must be prepared to constantly adapt to new production, logistics and organizational processes. In recent years, there has been a growing trend towards the re-localization of production (back-shoring), i.e. the return of production activities to their countries of origin after having been relocated elsewhere, which is made possible by technology offering savings on production and logistics costs. AM processes can be effectively applied within the Deming (PDCA: Plan- Do-Check-Act) cycle, a method used to improve product quality through four stages: *plan* (establish a plan and anticipated results); *do* (implement the change); *check* (evaluate progress done so far against the targeted goal); and *acts* (standardize and stabilize the process through appropriate review and assessment; restart the cycle). This cycle efficiently transforms ideas into finished products, improving quality and reducing production time and costs. The constant focus on manufacturing process efficiency and sustainability in recent years has stimulated a growing interest in AM techniques [2]. In the field of polymers in particular, laser-based powder bed fusion (PBF-LB) of polymers (PBF-LB/P) is becoming increasingly popular not only for producing not only prototypes, but also functional components with high dimensional accuracy for use in various sectors such as automotive, aerospace, and medical. This process involves a low-power CO_2 laser interacting with a bed of thermoplastic powder. As the laser melts the powder, the build platform moves downwards and the recoating system distributes a new layer of powder. This layer is then preheated for a few tens of seconds by thermal radiation from the heater elements located on top of the machine. This process is then repeated several times until the part is complete. Throughout, a low flow of nitrogen prevents oxidation of the powder, while additional heating elements around the build chamber and build platform maintain the environment at a temperature close to the sintering point of the processed material. An important aspect of this process in terms of product sustainability is the possibility of recycling the powder used in previous processes [3–5]. Upcycling is an evolution of the recycling concept [6], whereby material is recovered and improved to increase its value compared to its original or degraded state. It extends the useful life of powders used in PBF-LB processes, reduces waste and improves the efficiency of production. There are numerous economic and environmental advantages. From an economic perspective, it reduces the need to purchase new powders, which account for a significant proportion of production costs. Furthermore, by reducing demand for new powders, decreases reliance on energy-intensive and carbon-emitting processes for producing virgin powder. From an environmental perspective, upcycling promotes a circular economy model and reduces industrial waste. In this model, used powders are not disposed of as waste but are reintroduced into the production cycle. This reduces the environmental impact associated with producing and disposing of materials. This closed loop extends the useful life of powders and contributes to the sustainable management of resources. Upcycling powder also presents an opportunity to develop new business models. For instance, powder suppliers could provide remanufacturing services to their clients, establishing a closed loop where degraded powders are sent back to the supplier and subsequently sent back to the client for reuse. Suitable hydration techniques for older powder are often used [4]. This technique involves treating waste powder with steam and then drying it at temperatures ranging from 50 to 70 °C. This effectively lowers the polymer's molecular weight by reducing surplus carboxyl end groups. Consequently, this revitalised powder can be recycled in the PBF-LB/P process (patent DE102008024465). Powder modification for laser re-sintering requires exposure to water or steam to enhance the melting point and fusion enthalpy (patent US2004/0138344A1). Another method of recycling waste powder involves mechanical processing (such as grinding) combined with the simultaneous spraying of water and/or ethanol, followed by a drying phase (patent WO/2018/028728). These approaches reduce costs for manufacturers and generate new revenue for suppliers, enabling them to expand their service offering. However, careful management of powder traceability is required to implement this model, to ensure that it meets the required quality standards for end applications. Strict quality control is also required during the remanufacturing process, to ensure that recycled powders maintain their desired characteristics and are free from contamination or defects that could compromise the quality of the end product. Given the growing demand for additive manufacturing and increasing

environmental awareness, powder upcycling could become a vital part of the future of advanced manufacturing. However, a critical analysis of powder recycling in PBF-LB technology requires a more sophisticated approach than traditional economic models. Barclift et al. [7] has presented a cost model for the PBF-LB process with metal powder (PBF-LB/M) that based on the Sum-of-the-Year's Digits (SOYD) depreciation model, which allows a recovery value to be specified. There are three widely used depreciation models: Straight-Line (SLN), Double Declining Balance (DDB) and SOYD [7, 8]. The SLN model evenly distributes the cost of an asset throughout its useful life, assuming that the raw powder material depreciates at a constant rate, regardless of when it is used. However, this method does not take into account that new powder is more susceptible to chemical contamination and oxidation in the early stages. Therefore, a more appropriate depreciation model should reflect a rapid depreciation after the first few uses, followed by a slower decline as the powder is continuously reused. The DDB model uses an accelerated approach, whereby the asset's value declines rapidly initially and then more slowly in the later stages. However, as the DDB uses a fixed depreciation rate, it does not permit the specification of a salvage value. This means that manual adjustments are required to fit a specific scrap value. The SOYD model strikes a balance between the SLN and DDB models. In this model, the asset's value declines moderately in the early years and then more slowly as the material is continuously reused. While the initial depreciation in SOYD is slower than in DDB, this model allows a salvage value to be specified, providing greater flexibility for different types of materials. The basic assumption of the Barclift et al. model [7] is that powder depreciation follows a predictable and quantifiable trend when traditional accounting methods are used. However, this may be too simplistic a view, since it does not consider the complexities of the physical and chemical degradation to which the polymeric powder is subjected during production cycles. At an industrial level, the PBF-LB/P process never uses completely virgin powder, but instead mixes new powder with powder that has already been used in previous productions. This approach is motivated by economic and environmental considerations, as virgin powder is expensive and reusing powder significantly reduces operating costs and the environmental impact of the process. This is typically achieved by using a virgin-to-used powder ratio based on the feedstock powder manufacturers' recommendations [3]. Examples include a mixture of 70% virgin and 30% used [9], and a mixture of 50% virgin and 50% used [10]. However, these recommendations are arbitrary and could result in a heterogeneous powder mixture with widely varying constituent properties after several cycles of refreshing with virgin powder. During PBF-LB/P, only 3–20% of the powders are sintered [9–11], while the remaining 85–95% undergo physical and chemical degradation due to preheating, sintering, cooling and post-treatment [12, 13]. Due to thermal and mechanical cycling undergone during previous processing, recycled powder can exhibit significant variations in properties compared to virgin powder, and these variations can affect fundamental aspects such as the powder's bulk density, particle size distribution, flowability and sintering capacity. In addition, the powder is exposed to different temperature profiles during the process involving three phases (Fig. 1) [14]: pre-heating, building, and cooling. During the pre-heating phase, the powder layer is warmed to a temperature slightly below its softening point. This reduces the necessary laser power and minimises deformation of the component during cooling. This temperature, known as the bed temperature (T_B), remains consistent throughout the entire fabrication process. This isothermal state is generally achieved through ongoing exposure to infrared lamps and/or heating elements. During the building phase, the subsequent steps are carried out for each layer. First, the building surface is lowered by the thickness of the layer. Then, powder particles are distributed using a roller or a recoating blade. A laser beam then scans the powder layer to melt the exposed portions in line with the specified design. After exposure to the laser, powder particle fusion begins at temperatures exceeding the material's melting point. The component is then slowly cooled to the T_B temperature to facilitate solidification and fuse neighbouring particles together. Powder deposition typically takes place in an inert environment (nitrogen) to prevent contamination from the surrounding atmosphere during the procedure. During the cooling phase, the heat source is turned off and the powder bed slowly decreases in temperature until it reaches the temperature at which the part can be extracted (T_E).

Additionally, powder accumulating at the edges of the build bed and feed unit is exposed to lower temperatures than unsolidified powder in the centre of the build volume [3]. Numerous scientific studies [15–18] have addressed the issue of powder recycling in the PBF-LB/P technique, providing essential directives and guidelines on several crucial aspects in order to establish the optimal parameters for using recycled powders. This help to maintain high quality standards in the final product, maximize the efficiency of the production process, and develop more sustainable and competitive solutions. This study precisely addresses the need for sustainable, economically advantageous solutions for companies and customers alike by changing the cost model for products manufactured using PBF-LB/P technology. The aim of this study was therefore to modify the SOYD model to create an innovative, dynamic depreciation model for components produced

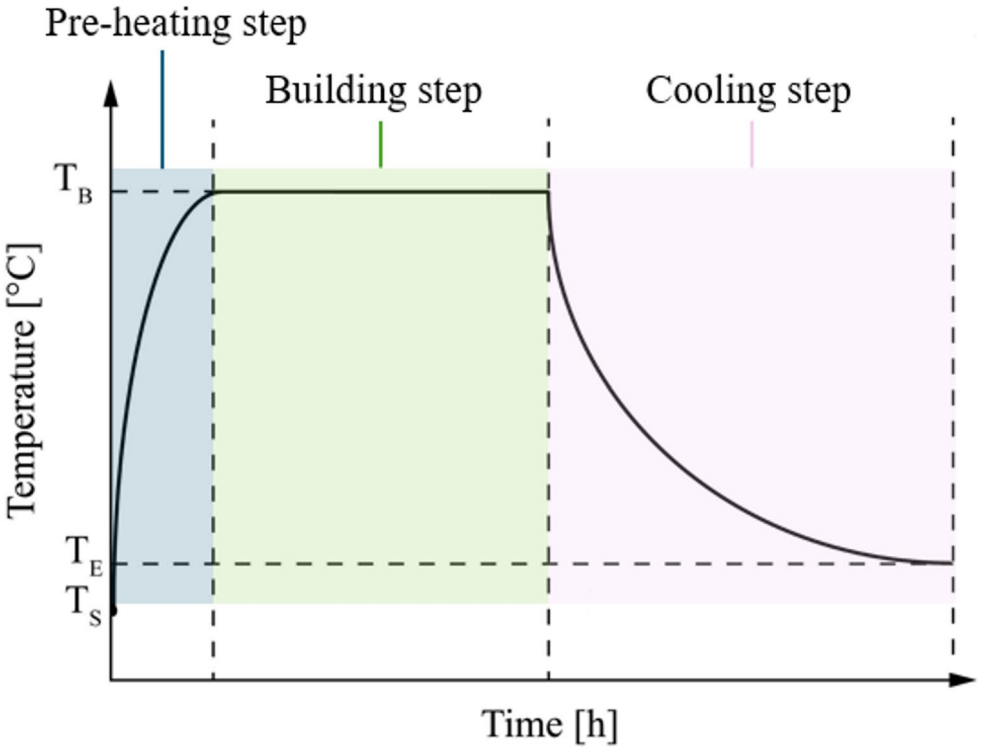

Fig. 1 Schematic representation of a temperature profile of PBF-LB/P process. T_s is starting temperature

using the PBF-LB/P process, in order to better represent the effect of degradation on the cost model. The material cost depreciation model has been applied to the manufacture of an integrated mechanical gear system. AM technologies have benefited the design and construction of robots and other mechatronic projects, as well as automotive and aerospace engineering, by enabling the creation of multi-joint mechanisms that integrate mechanical gears without the need for additional assembly operations. Advantages of these integrated systems include reduced assembly time and costs, quick evaluation of the overall working area and verification of gear or joint limits by determining any interference between parts. Polymer gears also offer unique advantages over metal gears in terms of sustainable production, including reduced costs and weight, high efficiency, quiet operation and operation without external lubrication. The production of an integrated mechanical gear system was carried out using virgin and mixed powders, with two scenarios being applied that had different residual economic values for the recycled polyamide 12 (PA12) powder. PA12 is one of the most widely used materials for PBF-LB/P due to its ideal sintering behaviour as a semi-crystalline thermoplastic polymer [19–21]. However, its properties degrade with reuse, which can affect the quality of the final product [22]. Current cost models do not account for these changes, which complicates the financial valuation of reused powders. Furthermore, most, if not all, of the studies reported in the literature on the degradation of this powder take 'cycle numbers' into account. However, these cycle numbers are not assigned a quantitative value in terms of hours of powder usage. The two scenarios presented in this study demonstrate how the method of calculating powder reuse — in cycles or hours of processing — can significantly impact the quality of parts produced, the cost of material and, consequently, the cost of the product.

2 Materials and methods

2.1 Degradation factors of PBF-LB/P/PA12 powder

Figure 2 illustrates the typical application of powder and the proportionate blending of fresh and recycled powder during PBF-LB/P processes. The first job performed on the machine uses only virgin powder. For subsequent jobs, the amount of powder to be added depends on the number of pieces to be built and the amount of powder loaded into the dispenser. If there is sufficient powder in the dispenser, only this powder is used. Otherwise, some powder must be added in the form of the sifted powder from the previous job (i.e. used powder). From the third job onwards, a mixture of powders will be used, consisting of a percentage of virgin powder (approximately 25–30%) and used powder ("refreshed powder" in this study), to which a percentage of powder previously mixed will be added in the various jobs.

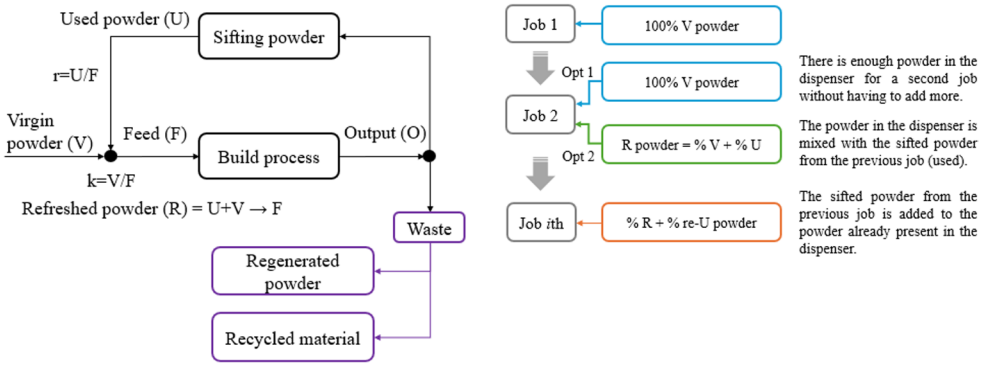

Fig. 2 Schematic sequence of powder usage in jobs. U, V, F and O represent the used powder, virgin powder, feed and outlet streams, respectively. The fraction of used and virgin material (refreshed powder) is defined by the ratios $r = U/F$ and $k = V/F$, related via the material balance, $F = U + V$

Waste is the residue from the sieve or separated powder that can be recycled for other processes [23, 24] or regenerated for use the refreshed powder [4]. The goal to incorporating virgin powder into the refreshed powder is to prevent further increases in the melting temperature (T_m) and to bring the thermal characteristics closer to those of the original powder. As Sanders et al. [25] highlighted, the largest increase in T_m occurs during the build phase of the first job, when all of the material is thermally 'unstressed'. After the second cycle, 50% of the powder has undergone two complete cycles, resulting in a reduced polycondensation rate. Adding 30% virgin powder prevents any further changes in T_m. Both used and refreshed powder exhibit an increased melting point related to the number of times the powder has been reused. For each successive build number, the melting range of the refreshed blend is slightly higher than that of the previously used powder. This difference between the refreshed and used powder can be explained by the fact that incorporating 30% new powder into the used material creates a mixture consisting of two distinct groups: fresh powder particles that tend to melt at lower temperatures and used powder particles that are expected to have a higher melting point. Consequently, there is a noticeable alteration in the shape and an expansion of the endothermic melting peak [26–29]. In the context of PBF-LB/P, an increase in the final melting point implies that more energy is required to completely fuse the powder particles. Therefore, if the build process parameters remain constant for each job, this could result in incomplete fusion and coalescence of the particles during sintering. This could lead to increased pore density, possible build failures and reductions in mechanical properties such as ultimate tensile strength (UTS) and Young's modulus [25].

The aged PA12 powder then undergoes a change in the level of properties. Dadbakhsh et al. [10] and Chen et al. [30] have argued that particle size changes little after ageing and remains arranged according to a Gaussian distribution centered at 50–60 µm. Meanwhile, particle sphericity – which measures how closely the shape approaches that of a perfect sphere – decreases with ageing. For instance, Yang et al. [31] conducted tests that showed 21% of particles in new powders had a sphericity between 0.9 and 1.0, compared to 16% in aged powders. Alo et al. [13] have explored phenomena such as the coalescence, agglomeration and fragmentation of PA12 particles. Their investigation revealed how the interactions between these internal dynamics and operating conditions can alter the size distribution and consequently affect the quality of the final manufactured product. Most particles, in both virgin and reused powders show signs of cracking.

Smooth and spherical powders are preferred for sintering as they reduce friction and mechanical interlocking during the layer-laying process. This leads to less agglomeration and better flow and packing behavior [32]. However, these powders are difficult to obtain: cracks in virgin powders are likely to be caused by the manufacturing process, while in reused powders they may result from prolonged exposure to high temperatures during the pre-heating, processing and cooling phases. Small satellite particles attaching to larger ones are due to the high cohesive forces and a "welding" effect caused by high temperatures in the processing chamber, which leads to the clustering of different fine particles within the cracks of the larger particles.

The size distribution of both virgin and reused powders was analyzed in terms of volume- and number-weighted distributions [10, 11, 13, 30]. Variations in size distribution due to recycling can arise from two opposing phenomena. The first is the partial joining of particles due to high temperatures in the processing chamber, leading to agglomeration and an increase in size due to cohesive forces between the particles. Conversely, abrasion between the particles can cause them to break into smaller fragments, particularly in particles with significant cracks. Therefore, reused powders show a higher proportion of fine particles than virgin powder. This is because sieving removes larger agglomerates, making fragmentation more prevalent than coalescence and agglomeration. Consequently, a higher proportion of fine particles is expected in powders with more reuse cycles.

Regarding the anisotropy of tensile strength, this increases with the number of recycling cycles, with significant differences between samples built in different directions. Yao et al. [17] investigated the effects of powder recycling on the uniaxial tensile properties of PA2200 samples (the trade name of EOS GmbH for PA12) printed in *xy/y*, *yz/y* and *yz/z* building orientations.

The tensile strength of PBF-LB/P samples made from new powders is lower than that of the initial set of recycled powders, and decreases gradually as the samples are made from the first to the eighth set of recycled powders. The mechanical properties of the polymer are influenced by the configuration and characteristics of the PA2200 molecules within the crystalline regions [12]. During the fabrication process, the development of larger and more intricate molecular structures in the recycled powders enhances intermolecular interactions, ultimately boosting the tensile strength of the PBF-LB/P components [33–35]. However, recycled powders have a higher melt viscosity than new powders due to thermal effects [36]. Residual pores of various morphologies are present [37, 38]. An increase in recycling cycles leads to a decline in the density of PBF-LB/P components, resulting in wider spread of voids and a reduction in tensile strength. Therefore, all these factors contribute to a decrease in tensile strength. Initially, as the duration of recycling increases, the anisotropy of tensile strength in PBF-LB/P samples also rises, but then a slight change occurs. There is not a significant difference in the tensile strength of PBF-LB/P samples based on different building orientations between fresh powders and third-generation recycled powders. However, an anisotropic behaviour in tensile strength is observed between the fourth and eighth generations of recycled powders, where the tensile strength in the *yz/z* build direction is somewhat lower than in the other two directions due to weak interlayer bonding.

2.2 Proposed cost model in PBF-LB/P process

In the literature, there are different cost models [39–44] and ways to calculate the build time [40, 44–47] in the PBF-LB process. In general, it is noted that the process can be divided into three phases: the pre-build, build and post-build phases. Consequently, the cost can be divided into three items, each corresponding to a phase of the process. The developed cost model focuses mainly on the build phase. To calculate the build cost, costs are grouped into three categories (Eq. 1):

$$C_{build}(p_i) = C_{buid-Machine}(p_i) + C_{build-Material}(p_i) + C_{build-Depreciation}(p_i) \quad (1)$$

Machine costs ($C_{buid-Machine}$) include costs (Eq. 2) associated with machine set-up (cleaning, machine preparation, etc.), the printing phase and machine downtime, i.e. before and after the printing phase in which there is a time required to heat the process chamber (warm-up time) and a time taken to cool the process chamber at the end of the job (cool-down time):

$$C_{build-Machine}(p_i) = C_{Machine_setup}(p_i) + C_{Machine_operation}(p_i) \quad (2)$$

$$C_{Machine_setup}(p_i) = (C_{op} + C_{AM}) \bullet \frac{T_{setup}}{\sum_i N_i} \quad (3)$$

Where

- C_{op} is the operator's hourly rate;
- C_{AM} is the direct hourly cost of the AM system and is the sum of the hourly energy consumption costs and machine maintenance costs;
- N_i is the quantity of parts with *i*th geometry as previously described;
- T_{setup} is the time for setting up the machine.

$$C_{Machine_operation}(p_i) = T_{build} \bullet C_{AM} \quad (4)$$

Where T_{build} is the total time needed to build a single part in a job. To get a true value, the value obtained from the PBF-LB/P machine software should be entered. Otherwise, a way to calculate it approximately is the algorithm proposed by Rickenbacher et al. [41]

$$T_{build}(p_i) = \frac{T_{idle}}{\sum_i N_i} + T_{exp} \bullet \sum_i (N_i \bullet V_{tot,i}) + T_{recoat}(p_i) \quad (5)$$

Where T_{idle} is the time when the AM machine is inactive (e.g., heating, cooling), T_{exp} is the time that the laser takes to sinter the powder, $V_{tot,\,i}$ is the total volume of the part for *i*th geometry, and T_{recoat} is the time needed to distribute a new layer of powder to be sintered.

The cost per part ($C_{build-Material}(p_i)$) is given by Eq. 6:

$$C_{build-Material}(p_i) = M_i \bullet C_{m,u} \quad (6)$$

Where M_i is the mass of a part with *i*th geometry and $C_{m,\,u}$ is the cost of the powder feedstock that has been used in *u* build cycles.

To evaluate the cost of the powder feedstock, it is necessary to take into account the recycling of the material which can penalize the properties of the parts produced.

In the SOYD depreciation model, the calculation is based on the cost of the asset (virgin powder, $C_{m,v}$), the salvage value (or residual value, S), i.e. the expected proceeds from the sale or scrapping of the asset at the end of its useful life, and the asset's useful life. Since the initial reuse cycles involve faster degradation, followed by a phase in which the already degraded powder loses value less evidently, it would be useful to introduce a degradation acceleration coefficient in the early stages of reuse, in order to adapt the SOYD model and reflect these dynamics. It is essential to calculate the overall loss of value of the powder during reuse. To determine the residual value of polymer, two possible scenarios can be considered:

1. *Chemical and physical degradation*: with increasing reuse cycles, PA12 can accumulate oxides and other chemical impurities that make its reuse difficult without significant regenerative treatment. Therefore, the S may be close to zero if one considers that the powder is no longer suitable for producing parts with stringent mechanical requirements. This degradation could be represented by a faster lowering of the $C_{m,u}$ value, i.e. the cost of the powder that has been used u times, and in this respect a degradation acceleration coefficient α_u could be introduced to alter the rate at which $C_{m,u}$ decreases:

$$C_{m,u+1} = C_{m,u} - \alpha_u \bullet (C_{m,v} - S) \bullet \left(\frac{U_{max} - u + 1}{\frac{U_{max}(U_{max}+1)}{2}} \right) \tag{7}$$

Where α_u is a factor that may be greater than 1 to reflect a more rapid degradation of PA12 in the first cycles, and U_{max} is the maximum number of build cycles or number of hours for which a powder can be used in a PBF-LB machine.

2. *Market for the waste material*: if there is a market for degraded powder, e.g. as a filler for composite materials or for applications that do not require high performance, the residual value may not be zero, but it would still be very low compared to the initial value of virgin powder. In the PBF-LB/M model, residual value is a crucial parameter. If it were very low compared to the initial cost of virgin powder, the decrease in powder cost after each cycle of use would be more pronounced. This would mean that the powder would lose value more quickly, as the model reflects the fact that it is losing most of its utility. It may be necessary to adapt the depreciation formula to handle situations where the residual value becomes practically zero after a certain number of cycles. Where it is recognised that the powder has no market value, even for secondary applications, the residual value could be set to zero to reflect the powder's unusability. This implies that the powder's cost will drop completely to zero beyond a certain critical point ($u_{critical}$), indicating its total loss of value.

$$C_{m,u+1} = C_{m,u} - (C_{m,v} - S) \bullet \left(\frac{U_{max} - u + 1}{\frac{U_{max}(U_{max}+1)}{2}} \right), \quad for\ u < u_{critical} \tag{8}$$

$$C_{m,u+1} = 0, \quad for\ u > u_{critical}$$

In addition, the depreciation of PA12 must take into account the *costs associated with powder replacement* (Eq. 9). If the powder is deemed unusable after a certain number of cycles, the depreciation cost must be distributed over a limited number of cycles, thereby increasing the cost per cycle. Equation 9 calculates the depreciation cost by distributing the powder loss over all parts produced during the construction cycle. For PA12, the $C_{m,u} - C_{m,u+1}$ differential is likely to be high in the initial cycles due to rapid degradation, leading to a significant increase in depreciation costs per manufactured part. One possible approach would be to use a non-linear function to more accurately reflect the non-constant loss of value of the powder, which initially accelerates, then stabilises, and then accelerates again towards the end of its useful life:

$$C_{build-Depreciaion}(P_i) = \frac{M_i}{\sum_i (N_i \bullet M_i)} \bullet (M_F - \sum_i (N_i \bullet M_i) \bullet (C_{m,u} \bullet e^{-bu} - C_{m,u+1})) \tag{9}$$

Where N_i is the quantity of parts with the ith geometry, M_F is the amount of powder loaded into the feed calculated as the product of density and building volume. The parameter b determines the rate of depreciation, while e^{-bu} is a decreasing exponential function that reduces the value of the powder non-linearly. Lopes et al. [22] demonstrated that material degradation during the PBF-LB/P process impacts the mass and mechanical properties of the components, resulting in an exponential loss of decay properties up to 50% of the initial properties. They tested the feasibility of using Bernardo's Eqs [48, 49]. to measure the decay of mechanical properties in the PBF-LB/P process. The property values after the first, second, ith and nth process steps when no virgin polymer is added ($k = 0$) are represented by P_0, P_1, $.P_i$, ., P_n. Curves representing the variation of P_n in relation to the number of cycles (usually known as degradation curves) are of great importance in refreshed studies. Equation 12 relates to the linear law of mixtures with loss of exponential decay properties:

$$\frac{P_n}{P_0} = \frac{k + (1-k)^{n+1}\left(e^{-bn} - e^{-b(n+1)}\right)}{1 - (1-k)e^{-b}} \tag{10}$$

In case of an exponential decay to an asymptotic value, the Eq. 10 is modified as follows:

$$\frac{P_n}{P_0} = \frac{P_a}{P_0} + \frac{a_0}{P_0} \bullet \frac{k + (1-k)^n \left(e^{-b(n-1)} - e^{-bn}\right)}{1 - (1-k)e^{-b}} \quad (11)$$

Where P_a the asymptotic value and a_0 the difference between the original and the asymptotic value of the property.

For mechanical and geometric properties that can only be measured after production, P_0 cannot be determined in advance. For practical purposes, it is therefore assumed that P_0 coincides with P_1. When calculating the mass of the part (M_i), it is necessary to take into account the powder that is not perfectly sintered and will subsequently be eliminated by the post-process. This powder must be considered lost material α_{loss} [%]:

$$M_i = (1 + \alpha_{loss}) \bullet \rho \bullet V_{part_i} \quad (12)$$

Therefore, to optimise the use of refreshed powder in PBF-LB/P processes, it is crucial to determine an accurate residual value that reflects the powder's degraded quality following several cycles. It is also crucial to manage the level of material degradation correctly, as this directly affects the calculation of depreciation costs.

2.3 Validation cost model

As mentioned above, in order to optimize the use of refreshed powder in PBF-LB/P processes, it is crucial to determine an accurate residual value. To achieve this, the issue of shrinkage defects in the PBF-LB/P process was examined, taking into account the practical implications for commercial users. The experimental design therefore takes a rigorous approach, scientifically evaluating shrinkage while reflecting realistic commercial operating conditions. For example, 30% virgin powder is used instead of the 50% typically specified by manufacturers of such production systems. This approach aims to mitigate some of the issues that arise during technology transfer, i.e., when results are transferred from idealized laboratory conditions to practical production environments. A series of components intended for commercial applications were used as reference parts for shrinkage evaluation in order to have more realistic values for evaluating production and therefore the effect on material costs. In particular, an integrated mechanical gear system was produced in two configurations: a simple shaft-wheel system and a gearbox (Fig. 3).

Two different uses of the powder were adopted for these two configurations (Fig. 4). Specifically, the first cycle of the shaft-wheel system was performed using 100% virgin powder, followed by subsequent cycles using refreshed powder (30% virgin powder and 70% used powder). After the initial build cycle, the unsintered powder surrounding the printed parts was removed, sieved and mixed to ensure uniformity. For the gearbox (Fig. 3b), the subsequent cycles were performed without adding virgin powder. Therefore, only the un-sintered powder present around the printed parts was removed and sieved after the initial cycle with virgin powder. Both the shaft-wheel system and the gearbox were manufactured using PA2200 powder (EOS GmbH's trade name for PA12). According to the

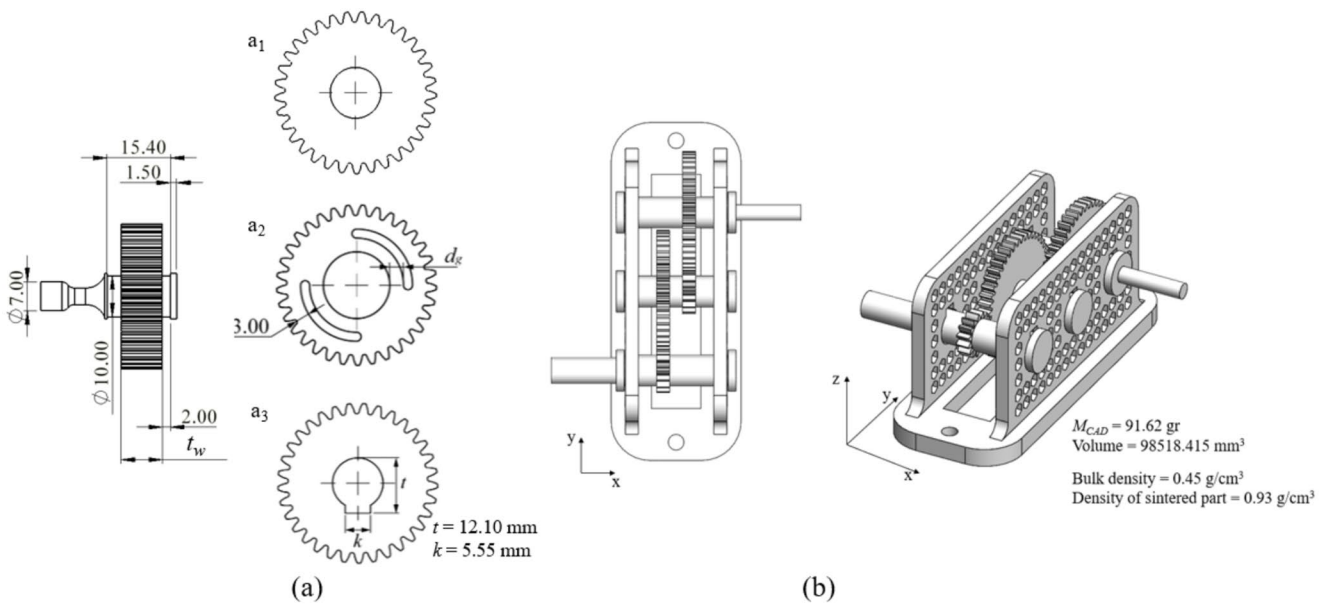

Fig. 3 Integrated mechanical gear design. (**a**) Shaft-wheel system with different wheel designs: (a_1) with standard geometry, (a_2) with slots, (a_3) with a groove between wheel and shaft. (**b**) Gearbox

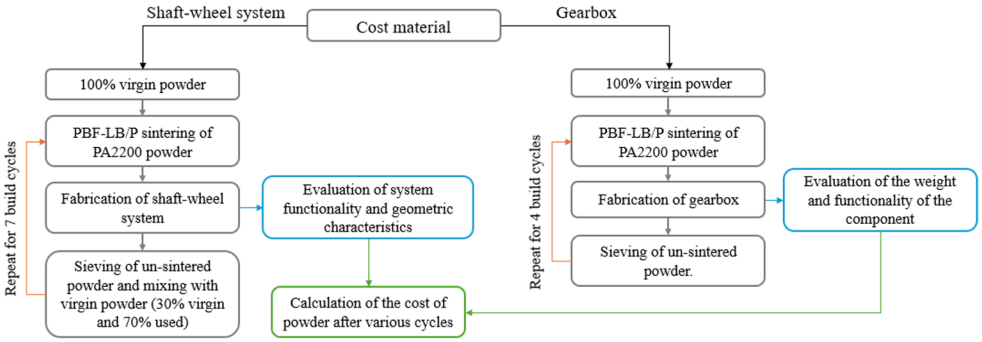

Fig. 4 Data creation flowchart for cost material validation

manufacturer's instructions, the PA12 powder is stored in closed bins in in a temperature- and humidity-controlled warehouse at a temperature of 23 °C ± 2 °C and an atmospheric humidity of 45% ± 5%.

In the shaft-wheel system (Fig. 3a), the diameter of the shaft was chosen as 10 mm based on the results of a previous study [3]. Secured in place between two collars fixed on the shaft, the wheel is prevented from detaching during locking tests. The collars are adequately spaced to enable access for inspecting and maintaining the shaft-wheel connection from both sides. They also allow for manually removing or shot-blasting any non-melted powder that may become trapped within the gaps. The shaft-wheel system design is characterized by fixed and variable parameters. The fixed design parameters are the root circle diameter (d_f = 30.5 mm), the addendum diameter (d_a = 35 mm), the total number of teeth (module m = 1), the clearance (c = 0.55 mm), the inner diameter (d_i = 4 mm), and the shaft diameter (d_s = 10 mm). The wheel thickness (t_w) and the distance (d_g) between the internal diameter and the slots (Fig. 3a_a_2) are considered variable design parameters. Three values were chosen for the t_w,: 8 mm, 10 mm, and 14 mm. Two values were chosen for the d_g: 2.5 mm and 3 mm. The relationship between d_s and t_w enables us to examine how thermal masses, which absorb heat, affect the closure of the gap and introduce a certain inertia to temperature variations. The presence of these thermal masses may also enhance the sintering process, affecting the wheel's rotation relative to the shaft. For this reason, the standard wheel design (Fig. 3a_a_1) was modified to create two new designs: one with two through slots to reduce the mass in the area between the wheel and the shaft (Fig. 3a_a_2), and one with a groove between the shaft and the wheel (Fig. 3a_a_3), similar to drive wheels. The groove has been designed to be rectangular in order to reduce the typical stair-case effect of the process. A hexagonal hole has been designed in the opposite end of the shaft to accommodate an M6 Allen key. This can be used to rotate the shaft and unlock the mechanism after cleaning. Two building orientations have been chosen: "horizontal", with the shaft-wheel axis parallel to the construction axis (z-axis), and "vertical", with the shaft-wheel axis perpendicular to the construction direction.

Twelve combinations of the shaft-wheel system were replicated twice and positioned at two different heights within the build chamber: 5 mm (level 1) and 200 mm (level 2) from the build platform. This resulted in a total of 48 components. The samples were positioned uniformly along the x- and y-axes to avoid areas of heat accumulation. Two different heights were considered in order to analyze the effect of z-compensation on part shrinkage during the cooling phase. This is evaluated during thermocouple calibration using a process known as a "quality job". This z-compensation is adjusted linearly between a minimum and maximum z value. To mitigate shrinkage problem, it is common practice to apply an adjustment constant to production parts, making them slightly larger in order to compensate for subsequent shrinkage. This value is known as the 'scaling factor' and is supplied by machine manufacturers for various machine configurations and materials. Since parts in the PBF-LB/P process are built layer by layer, the material shrinks differently in the x and y directions than in the z direction. Therefore, each scale value must be calculated and applied separately to the build. However, discrete scaling factors assume linear shrinkage across the entire part, which may not be valid for the z-axis [50]. The following scaling factors were obtained from a quality job carried out using virgin powder: 3.35% and 3.27% for the x- and y-axes, respectively. Along the z-axis, the scaling factor varied linearly from 2.6% at z = 0 mm to 2% at z = 300 mm. The job height was 196.90 mm, with the same job being produced for seven cycles. X-ray CT scanning (GE Phoenix vjtomejx s) was performed to examine the gear non-destructively. The scan parameters were a voltage of 100 kV, a current of 50 mA and a voxel size of 50.224 mm. GOMInspect software was used to compare the CAD model with the 3D model obtained from the CT scan. For the gearbox, the same component was produced in each print cycle, for a total of four components corresponding to the four production cycles. The job height was 57 mm.

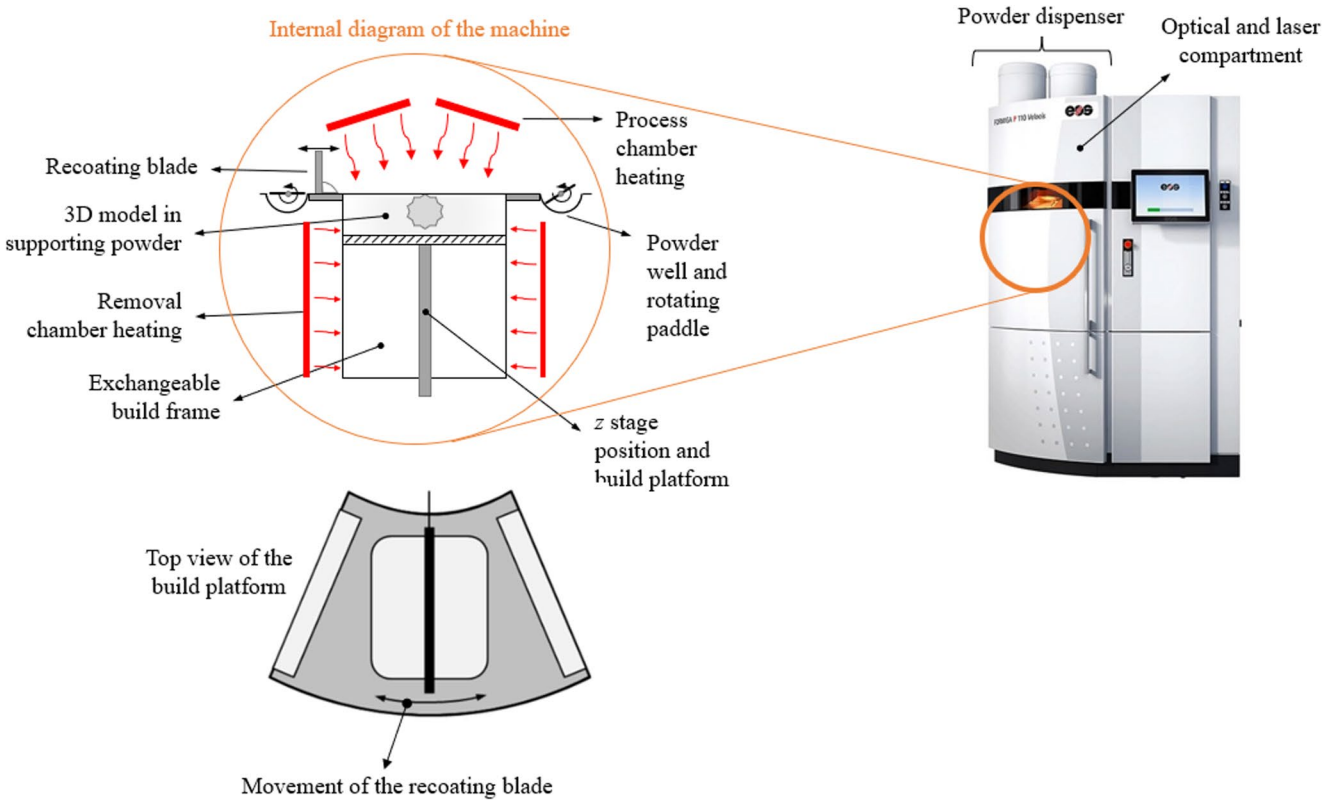

Fig. 5 Schematic representation of the EOS Formiga P110 Velocis

The parts were produced using an EOS FORMIGA P110 Velocis machine (Fig. 5), which has a theoretical build volume of 200 mm x 250 mm x 330 mm. However, a portion of this build volume, equivalent to 40 mm x 30 mm x 330 mm, is occupied by the radiation pyrometer, which measures the temperature of the powder bed for each layer. Therefore, this portion is excluded from the working volume. The machine is installed in a room with temperature and humidity control, as required by the manufacturer: a temperature of 23 °C and a humidity level of 45%. The parts were printed using the standard performance process parameters for PA2200 provided by the EOS GmbH: a laser power of 21 W, a scan speed of 2500 mm/s, and a hatching distance of 0.25 mm. The layer thickness was set to 0.10 mm and the waiting time between the end of a layer and the subsequent powder deposition was set to 5 s. The process chamber and removal chamber temperatures were set to 169 °C and 154 °C, respectively. After the production, the total cooling time was 4 h. A specific quantity of PA2200 powder is applied to the build chamber to create a homogeneous powder bed. The initial height of this layer depends on the PBF-LB/P system used. After the initial powder has been pre-heated, the build process begins with the heating phase. During this phase, layers of powder are applied to the build chamber without laser exposure. The build height of this phase varies, and in this study it is 5 mm. These layers act as thermal insulation, reducing heat transfer between the exposed component cross-section and the metal build chamber. Once all the layers of the component have been built, the cooling phase begins. During this phase, additional layers of powder are applied without laser exposure to create an insulating layer that prevents heat transfer from the molten components. These bottom and top insulating layers thus prevent unbalanced crystallization of the components, thereby preventing warping. After that, any loose powder was gently removed from the samples by shot-blasting with glass beads and compressed air, after which they were cleaned manually with a brush.

3 Results and discussion

3.1 Integrated mechanical gear

Starting with an analysis of virgin powder used without a mixer, and then with a mixer. Table 1 shows the data relating to the cumulative build time and weight of the four gearboxes produced. All parts exhibit a variation in weight, calculated as the product of density and volume. This 4.19 g variation in the first piece can be attributed to incompletely sintered powder in hard-to-reach areas of the piece. However, Lopes et al. [22] have highlighted that the mass

Table 1 Build time and weight of the gearbox produce in four job

Build cycle	Powder	Printed part name	Cumulative build time	Weight [g]
1	Virgin	G1	2h23min	95.81
2	Used	G2	3h22min	96.00
3	Used	G3	3h45min	96.05
4	Used	G4	3h52min	97.05

is higher for the horizontally produced samples. Some parts of the gearbox are built vertically and some horizontally. The weight increases slightly with each cycle, probably due to the ageing of the powder. The weight variations between the pieces are small and correspond to the variation in construction time. This is probably because the construction time is short, so the effect is less noticeable than in other studies where the times increases even double in the first two cycles [13].

The total time for the four jobs is 13 h and 23 min, to which the time taken for the powder to heat up and cool down should be added. For this number of hours, low powder degradation is visible in Fig. 6, which shows the virgin powder (Fig. 6a) and the used powder (Fig. 6b) after the four jobs. Both type of powder exhibit an irregular shape, with small satellites on the surface. In both types of powder, smaller particles of a lighter shade can be seen. Titanium dioxide (TiO_2) is added to PA2200 powder to improve its whiteness, flowability and absorbency. This compound also acts as a nucleating agent. The differential scanning calorimetry (DSC) thermogram for the powder is shown in Fig. 6c. The heating and cooling cycles are very similar, and the melting temperature reproduces the manufacturer's claims well. The sintering window for the virgin powder is approximately 12 °C, while for the used powder it extends up to 16 °C. The heat associated with melting also shows no significant changes after four cycles of use in the PBF-LB/P process, indicating insignificant degradation. During cooling, the behavior is perfectly reproducible.

Moving on to the analysis of the refreshed powder, Table 2 shows the average results of the effect of wheel thickness, orientation and powder on the shaft-wheel system. Three scenarios are considered with respect to the axial and rotational direction of the system: locked in both directions; unlocked in the axial direction only; and unlocked in both directions. Significant differences emerge when comparing the use of 100% virgin powder and refreshed powder. The wheel thickness and system manufacturing orientation affect the rotation of wheels with a diameter greater than 8 mm. If the system is built horizontally, rotation and axial movement relative to the shaft are blocked when the wheel is 10 mm thick. If the system is built vertically, the wheel exhibits axial movement when mixed powder is present. Inserting slots with a d_g value of 2.5 mm does not alter the outcome of the standard wheel design. However, increasing the d_g value by 0.5 mm enables a wheel made with refreshed powder to rotate and move axially on the shaft, regardless of orientation. In the case of virgin powder, however, the system remains blocked. With a wheel thickness of 14 mm, movement is permitted for wheels made with virgin powder if there is a groove, but not for those made with mixed powder. In addition to the typical staircase effect, the area between the wheel and the shaft is more rounded in vertically built wheels due to the partially sintered powder. This means that, while they can free themselves by creating an axial movement, they cannot rotate. Applying a sufficient force to break the weak links between

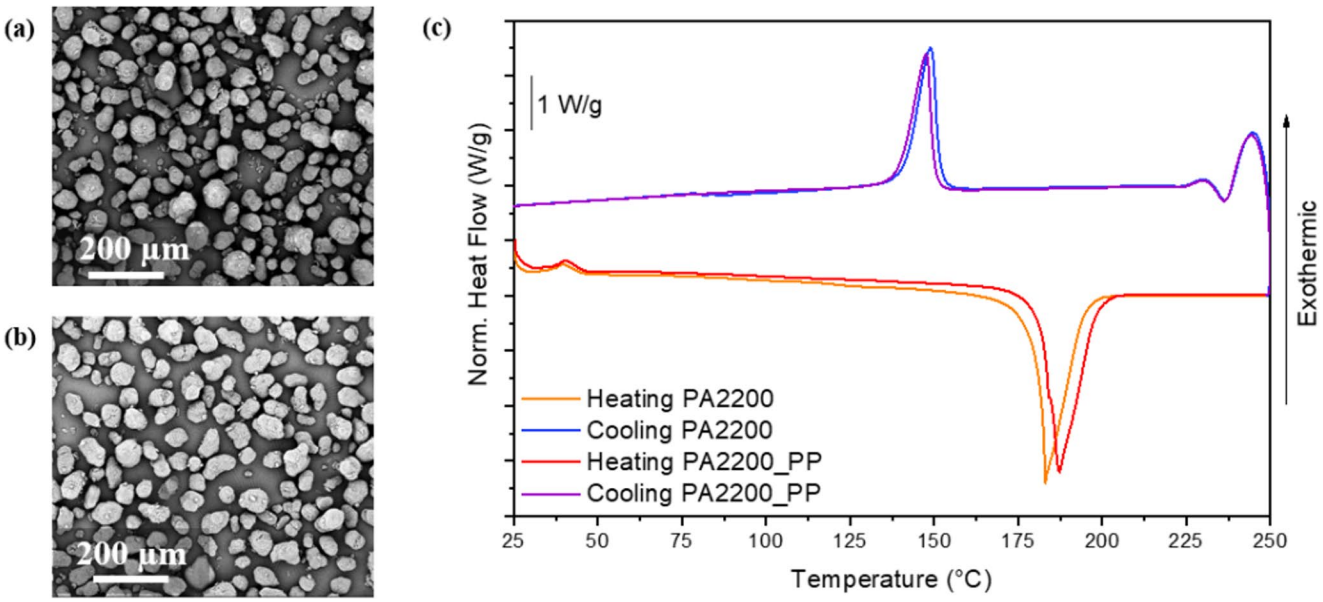

Fig. 6 (**a**) Virgin, (**b**) recycled powder, (**c**) DSC plot of the virgin and recycled powder

Table 2 Locked and unlocked shaft-wheel system. Legend: ○ 100% Virgin powder; ■ refreshed powder after approximately 42 h; ▲ refreshed powder after approximately 86 h

Level 1				Level 2			
Sample	Unlocked	Locked	Axial unlocked	Sample	Unlocked	Locked	Axial unlocked
$H1_8$	○ ■			$H1_8$	○ ■		
$H2_{10}$		○ ▲		$H2_{10}$	■	○	▲
$H3_{14}$		○ ▲		$H3_{14}$	■	○	▲
$V1_8$	○ ■ ▲			$V1_8$	○ ■ ▲		
$V2_{10}$		○	■	$V2_{10}$		○ ▲	■
$V3_{14}$		○	■	$V3_{14}$		○ ▲	■
Slot 1 (d_g = 2.5 mm)							
$H1_{8_s1}$	○ ■			$H1_{8_s1}$	○ ■		
$H2_{10_s1}$		○ ■ ▲		$H2_{10_s1}$		○ ▲	■
$H3_{14_s1}$		○ ■ ▲		$H3_{14_s1}$		○ ▲	■
$V1_{8_s1}$	○ ■ ▲			$V1_{8_s1}$	○ ■ ▲		
$V2_{10_s1}$		○ ▲	■	$V2_{10_s1}$		○ ■	▲
$V3_{14_s1}$		○ ▲	■	$V3_{14_s1}$		○ ■	▲
Slot 2 (dg=3 mm)							
$H1_{8_s2}$	○ ■			$H1_{8_s2}$	○ ■		
$H2_{10_s2}$	■	○ ▲		$H2_{10_s2}$	■	○ ▲	
$H3_{14_s2}$		○ ■ ▲		$H3_{14_s2}$		○ ▲	■
$V1_{8_s2}$	○ ■ ▲			$V1_{8_s2}$	○ ■ ▲		
$V2_{10_s2}$	■	○ ▲		$V2_{10_s2}$	○ ■	▲	■
$V3_{14_s2}$		○ ▲	■	$V3_{14_s2}$		○ ▲	■
Groove							
$H1_{8_g}$	○ ■			$H1_{8_g}$	○ ■		
$H2_{10_g}$	○	■ ▲		$H2_{10_g}$	○	▲	■
$H3_{14_g}$	○	■ ▲		$H3_{14_g}$	○	▲	■
$V1_{8_g}$	○ ■ ▲			$V1_{8_g}$	○ ■ ▲		
$V2_{10_g}$	○	▲	■	$V2_{10_g}$	○ ■	▲	■
$V3_{14_g}$	○	▲	■	$V3_{14_g}$	○	▲	■

the un-sintered particles and to overcome the friction force generated between the gear's faces and the un-sintered powder unlocks the system by imparting axial movement to the wheel on the shaft.

The wheels were analysed using a Ct scan and compared with the CAD models (Fig. 7). As can be seen in Fig. 7a and b, the standard design wheel has good dimensional accuracy when built with virgin powder, despite the different orientation. However, when 70% of the used powder mixed with the refreshed powder has been in use for over 42 h, various defects begin to appear. In particular, regardless of their orientation, the components exhibited more pronounced deformation in one direction than the other on the *xy*-plane. These deformations are more evident in wheels with slots and grooves, and they do not behave uniformly; that is to say, depending on their position on the level and on the plane, the deformations vary without indicating a preferential trend.

Nine 10 mm cubes were produced to better understand the phenomenon and positioned evenly on the plane, at the same distance from the z-axis of the wheels (levels 1 and 2). A total of 18 cubes were used. Cubes were chosen as their geometry provides a clearer picture of the shrinkage on the axles. Their smaller mass than that of the shaft-wheel system enables a better understanding of the factors involved in deformation beyond mass and powder age. These were produced using both virgin and refreshed powder. In the latter case, the cubes were measured after approximately 42 and 86 h of powder reuse. Table 3 shows the mean results. The standard deviation is indicated in parentheses. Figure 8 shows the position of the cubes in detail, as well as their relative shrinkage along the three Cartesian axes. In dimensional geometry, positive shrinkage means a shape reduces in size by contracting towards its centre. Negative shrinkage, often referred to as expansion or dilation with a negative factor, indicates that the shape is growing larger.

The cubes produced with virgin powder were found to be almost uniform in all three directions, with similar values at both levels. For the virgin powder, considering the *x*-axis, the largest deviations were found in the central part (cube 4 and 6) in both levels. However, for the refreshed powder, the behavior of the two levels is almost opposite after 42 h: in level 1, the cubes show a reduction in size except for cubes 5 and 8; in level 2 all the cubes show an increase in size along the axis. After approximately 86 h,

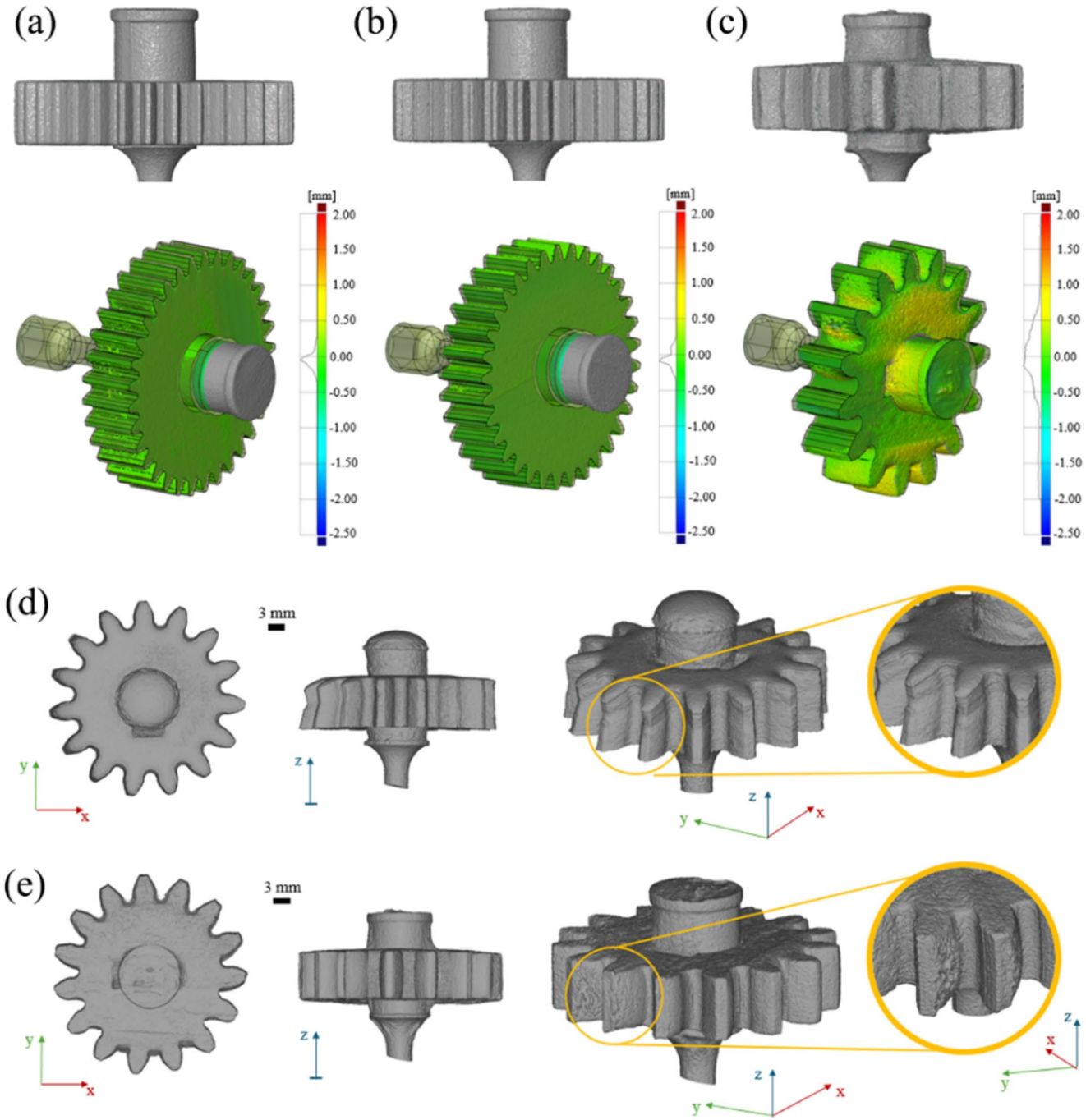

Fig. 7 Ct scan images. (**a-c**) Comparison with the CAD model: (**a**) Sample $H1_8$, virgin powder; (**b**) sample $V1_8$,virgin powder; (**c**) sample $V2_{10_g}$, refreshed powder, approximately 86 h. (d) Sample $H2_{10_g}$, (e) sample $V2_{10_g}$

Table 3 Dimensional accuracy of the cubes. Measurements are in millimeters. Nominal size of the cubes considering the scale factor: $x = 10.035$ mm, $y = 10.033$ mm, $z = 10.026$ for level 1 (scale factor 2.59) and z = 10.022 mm for level 2 (scale factor 2.2)

	Virgin			Refreshed − 42 h			Refreshed − 86 h		
	x	y	z	x	y	x	x	y	x
Level 1	10.04 (0.06)	10.05 (0.05)	10.00 (0.07)	9.96 (0.08)	10.04 (0.11)	9.91 (0.03)	9.99 (0.04)	9.98 (0.03)	9.95 (0.02)
Level 2	10.04 (0.06)	10.05 (0.05)	10.00 (0.07)	10.19 (0.03)	10.18 (0.03)	10.38 (0.07)	10.01 (0.06)	9.98 (0.05)	10.11 (0.04)

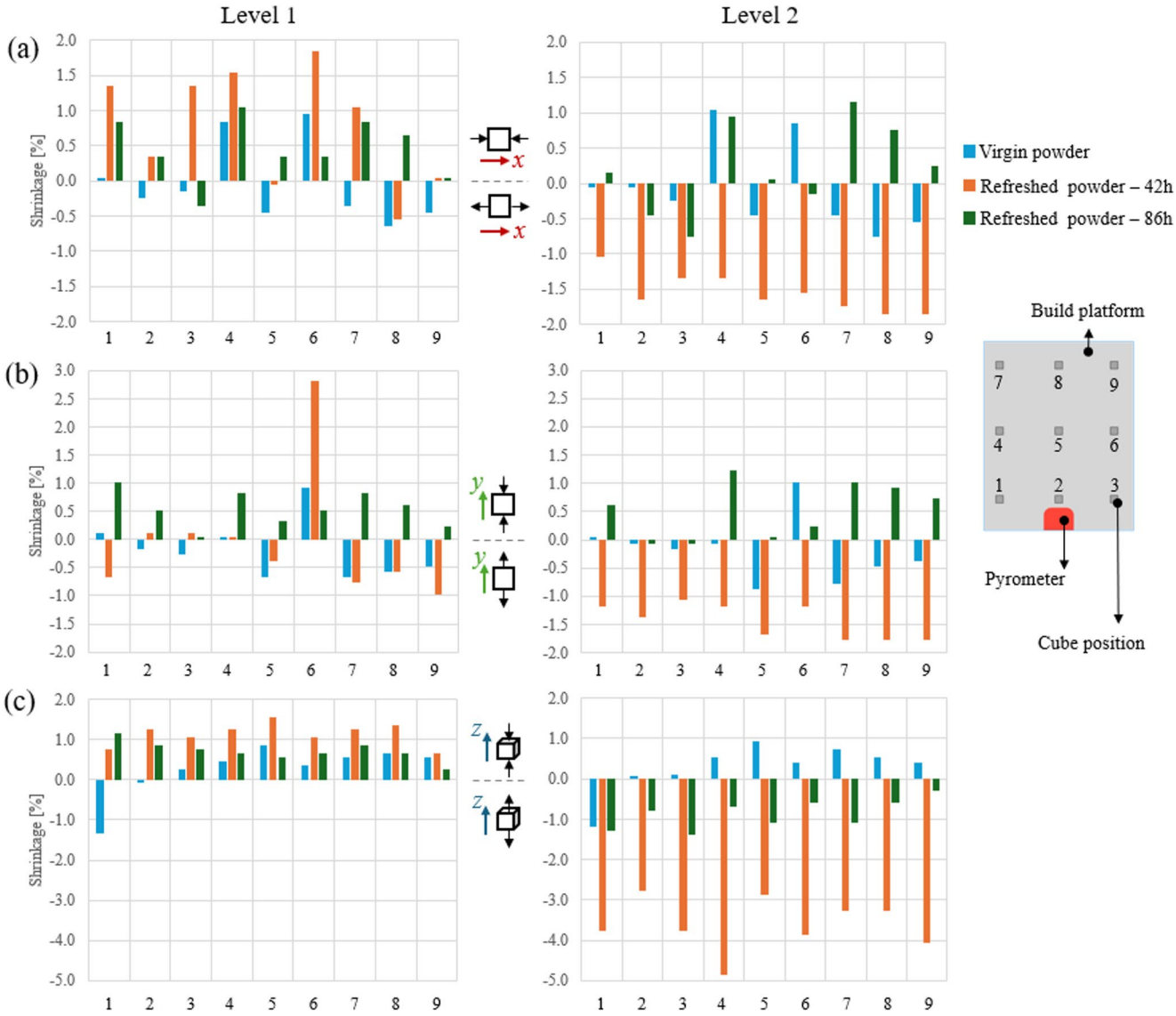

Fig. 8 Position of the cubes and their relative shrinkage with respect to the three Cartesian coordinates

the size effect becomes less pronounced, with the behavior of the two levels becoming more similar, except for cubes 2 and 6, which exhibit opposite trends. On the *y*-axis, the behavior is similar for both levels with the virgin powder. When using refreshed powder for more than 42 h, cube 6 shows the greatest deviation at level 1. Along with cubes 2, 3, and 4, it shows a decrease in size. At level 2, however, they all increase in size. As with the *x*-axis, the deviations are less pronounced when refreshed powder is used for 86 h than for 42 h, with few differences between the two levels. In general, slight differences were observed on the *xy* plane after 42 h, confirming that degradation occurs more rapidly in the initial reuse cycles, causing dimensional variations that remain more or less constant. On both axes, reusing powder for more than 42 h can lead to a reversal of the deviation compared to components produced with powder that has been used for less than 42 h. On the *z*-axis, the behavior between the two levels differs, except in the case of virgin powder. One possible explanation for this is the components' exposure over time. Components produced at the beginning of the process (level 1) are exposed to prolonged heating compared to those produced towards the end (level 2). Over the course of a full process, this results in several hours of additional heat exposure, which could alter the material's properties and cause greater shrinkage.

The effect of the mass of materials in the upper layers of the part must be taken into account. This exerts a compressive force on the lower powder layers, which promotes shrinkage. Since the wheels have a greater mass than the cube, the effect of non-uniform shrinkage (also known as "anisotropic shrinkage") is more evident. Due to its inhomogeneous nature, shrinkage varies more in the y-direction

than the nominal size of a sample [51]. This inhomogeneity is influenced by thermal gradients and coating movements. The thermal gradient during the forming and cooling process varies according to the lengths of the strips in the sample and the age of the powder. Considering the variation in energy density – defined as the ratio of laser power to the product of scanning speed, hatch distance and layer thickness – a hatch with a longer scanning vector length has a longer delay time between consecutive exposures of the same point. Conversely, a shorter length has a shorter delay time [52]. The delay time is calculated as the ratio of the distance travelled by the laser beam to scan two consecutive points to the scanning speed. This is compounded by the effect of variation in solidification due to the state of the powder. Shrinkage in the longer regions differs significantly from that in the shorter regions because shrinkage in large geometries is delayed by internal stresses [53]. Consequently, the 0.5 mm difference in thickness between the two wheels in the slot areas results in different solidification and cooling times, which affects geometric accuracy. Considering the movement of the recoater, this occurs in the *x*-direction of the machine. The amount of powder, and therefore its weight, varies in the *y*-direction as it is deposited during movement from one side of the print platform to the other. The powder is heavier at the start of the application process and lighter at the end. According to the data reported in the literature [16], the molecular weight of PA12 varies with build time. With build times of 10.6 and 26.6 h, the average molecular weights of PA12 are 49,400 g/mol and 61,100 g/mol, respectively (new powder shows an average molecular weight of 32,900 g/mol). During sintering, the area tends to be lower than the powder bed due to gravity and its weight. Therefore, the layer height differs in different areas of the bed, depending on the state of the powder used. The pressure exerted by the recoater on the new layer varies because the blade moves in the opposite direction in the next layer; therefore, there is no uniformity in the *y*-direction. This non-uniform shrinkage can be reduced by adjusting the scaling factors along the three axes according to the age of the powder. However, this approach has its limitations. While producing calibration components for the *x*- and *y*-axes is quick and cost-effective, the same cannot be said for *z*-axis. For the *x*- and *y*-axes, the components are produced parallel to the powder bed, requiring only a few layers of material and reducing production times. In contrast, calibrating the *z*-axis requires a complete production cycle, which can be costly in terms of materials depending on the print volume. Consequently, this approach is expensive and time-consuming, and may be considered commercially unviable.

3.2 Effect on costs

The results presented so far for the analyzed systems have highlighted the issue of only considering the number of cycles rather than the number of hours of powder usage. Several papers have explored the effect of ageing on the reuse of PA12 powder in multiple production cycles without refreshing the powder [11, 16, 17, 54, 55]. These studies have shown that with increased powder reuse results in higher melt viscosity, ultimately leading to reduced part density and strength. However, these studies either do not report the total cumulative production time [11, 55, 56], or use production times that are much shorter than those commonly used in industry [16, 29]. Therefore, the calculation should be made considering the number of hours. For the PA2200 powder used in this study, which costs 68 €/kg, the value of the powder feedstock using SOYD (Eq. 6) would differ depending on whether the maximum number of cycles or the maximum number of hours of use is considered. Table 4 shows the cost results for scenario 1($S = 0$) and scenario 2 ($S = 26$ €/kg) for the shaft-wheel system. Prior to each process, the PA2200 raw material was refreshed with 30% virgin powder, resulting in an extended cumulative production time of approximately 99 h, including cooling. The percentage of sintered powder in each job is 3.6%. The percentage of lost powder – that is, powder that adheres to the parts due to heat but does not sinter – has been estimated and reported in Table 4.

The results (Table 4; Fig. 9) emphasise the importance of understanding how the powder behaves in terms of its

Table 4 A numerical example of the cost of the powder after the first use according to the two possible scenarios

α_u			Scenario 1	Scenario 2			Scenario 1	Scenario 2
	U_{max} [cycles]	u [cycle]	$C_{m,\,u+1}$ [€]	$C_{m,\,u+1}$ [€]	U_{max} [h]	u [h]	$C_{m,\,u+1}$ [€]	$C_{m,\,u+1}$ [€]
-	7	0	68.00	68.00	100	0	68.00	68.00
1.5		1	42.50	56.00		14	66.24	67.16
1		2	27.93	45.50		28	65.56	66.44
0.8		3	18.21	36.50		42	66.20	64.93
0.6		4	12.39	29.00		56	66.76	63.54
0.4		5	9.47	23.00		71	67.26	62.27
0.4		6	7.53	18.50		85	67.33	61.12
0.4		7	6.56	15.50		99	67.41	60.09

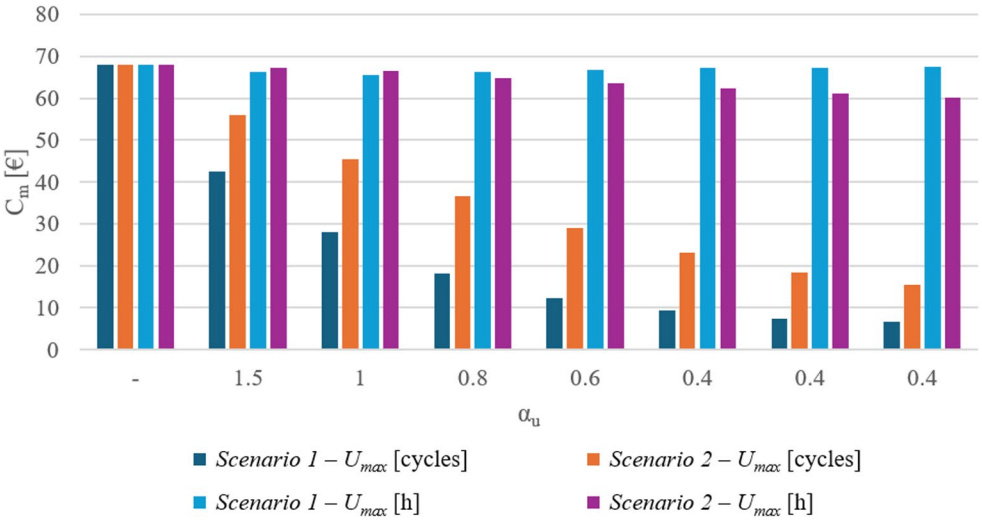

Fig. 9 Cost comparison for the two scenarios

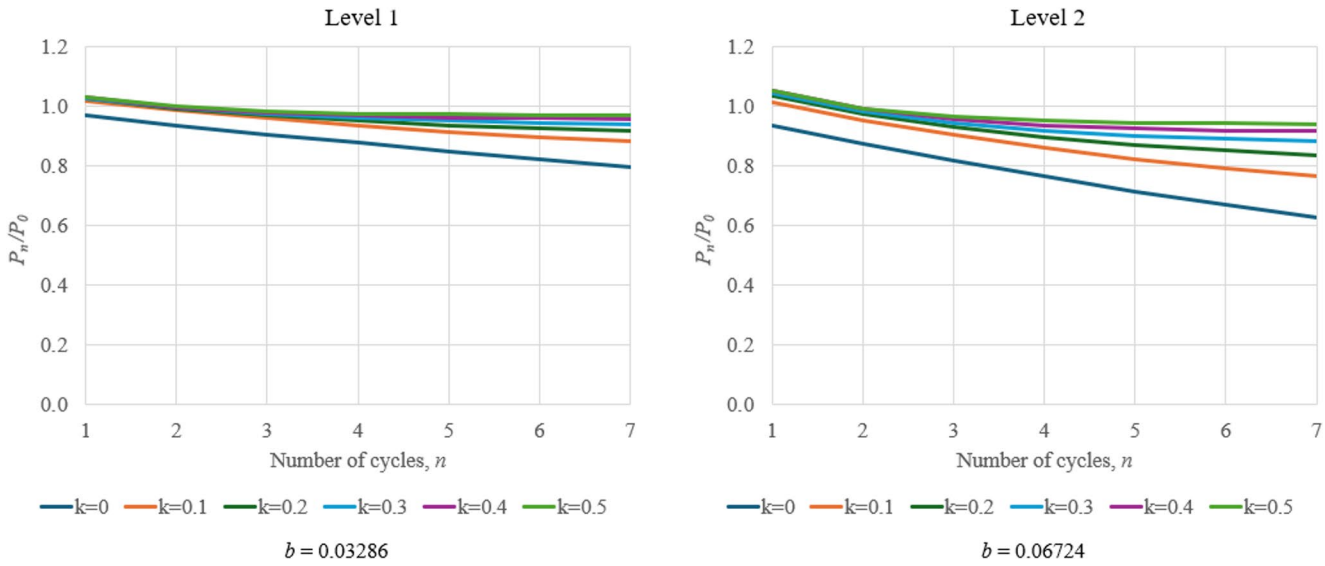

Fig. 10 The dependence of the volume shrinkage of shaft-wheel system parts on n for different k values

mechanical and geometric properties, and correlating this with usage time. This is necessary in order to create a more realistic cost model that is consistent with the process parameters and the PBF-LB/P system used. Considering only the number of cycles does not provide accurate information on degradation and can lead to an underestimation of the cost of the material used to produce the part.

At an industrial level, the material cost calculation for producing a part is usually carried out before construction begins. Therefore, the weight value of the part and the powder quantity loaded into the feed are based on the product of volume and density. Then, Eq. 12 can be used to take this difference in weight into account at an economic level thanks to the coefficient α_{loss}. This coefficient can be estimated experimentally. Considering the gearbox and using an α_{loss} value of 4% and $b = 0.1334$, the depreciation cost of the gearbox in cycle 1 would be € 94.84, increasing as the powder's usage cycle increases. The value of b significantly affects the calculation and is therefore an important factor in evaluating the depreciation cost: reducing the value of b by 0.01 lowers the depreciation cost from € 94.84 to € 80.60. Figure 10 illustrates the effect of the value of b. For the shaft-wheel system, the real volumes were calculated and the value of b obtained by considering two different levels. A single theoretical curve was created to predict the average volume change due to shrinkage, based on the number of building cycles (n) and the virgin PA2200 material ratio in the blend (k), for a fixed value of b (Fig. 10). The number of cycles corresponds to the number of hours shown in Table 4. For example, $n = 1$ corresponds to 14 h, $n = 2$ to 28 h, and so on. Different volume shrinkage of the parts at the two z levels determine different value of b, which affect the depreciation cost: there is a difference of approximately 2 euros between the two levels.

4 Conclusion

In the PBF-LB/P process, polymer powders such as PA12 tend to degrade when exposed to high temperatures, resulting in non-linear degradation. The cost models available in the literature for this process do not identify or quantify this degradation, even though it affects the characteristics of the final parts. The proposed model considers the reduction in the economic value of the powder and can also incorporate material quality parameters. The study emphasised the importance of scientific quantification based on hours rather than generic cycle numbers, to improve understanding the impact of powder reuse on components more similar to those produced industrially. Applying the SOYD model with the necessary adaptations enables effective management of the economic lifecycle of powders, minimizing waste and ensuring sustainable production. Adopting a dynamic amortization model supported by real data on powder degradation would be a significant step towards more efficient and sustainable resource management in industrial additive manufacturing.

Acknowledgements The authors would like to thank Eng. Mariantonietta Piconio for her support with the bibliographic research and development of the cost model.

Author contributions All authors contributed to the study conception and design. Material preparation, data collection and analysis were performed by Flaviana Calignano and Giovanni Marchiandi. The first draft of the manuscript and the revised version were written by Flaviana Calignano and all authors commented on previous versions of the manuscript. All authors read and approved the final manuscript.

Funding Open access funding provided by Politecnico di Torino within the CRUI-CARE Agreement. Financed by the European Union – NextGenerationEU (National Sustainable Mobility Center CN00000023, Italian Ministry of University and Research Decree n. 1033–17/06/2022, Spoke 11 – Innovative Materials and Lightweighting). The opinions expressed are those of the authors only and should not be considered as representative of the European Union or the European Commission's official position. Neither the European Union nor the European Commission can be held responsible for them.

Declarations

Competing interests The authors have no relevant financial or non-financial interests to disclose.

Open Access This article is licensed under a Creative Commons Attribution 4.0 International License, which permits use, sharing, adaptation, distribution and reproduction in any medium or format, as long as you give appropriate credit to the original author(s) and the source, provide a link to the Creative Commons licence, and indicate if changes were made. The images or other third party material in this article are included in the article's Creative Commons licence, unless indicated otherwise in a credit line to the material. If material is not included in the article's Creative Commons licence and your intended use is not permitted by statutory regulation or exceeds the permitted use, you will need to obtain permission directly from the copyright holder. To view a copy of this licence, visit http://creativecommons.org/licenses/by/4.0/.

References

1. Calignano F, Mercurio V (2023) An overview of the impact of additive manufacturing on supply chain, reshoring, and sustainability. Cleaner Logistics and Supply Chain. https://doi.org/10.1016/j.clscn.2023.100103
2. Adin MŞ (2024) A Study on Additive Manufacturing Processes, Standards and Mechanical Properties. Post-Processing Parts Components Fabr by Fused Depos Model Tech Adv 213–231. https://doi.org/10.1201/9781032665351-15/STUDY-ADDITIVE-MANUFACTURING-PROCESSES-STANDARDS-MECHANICAL-PROPERTIES-MEHMET-
3. Calignano F, Bove A, Mercurio V, Marchiandi G (2023) Effect of recycled powder and gear profile into the functionality of additive manufacturing polymer gears. Rapid Prototyp J. https://doi.org/10.1108/RPJ-06-2023-0199
4. Olejarczyk M, Gruber P, Gazińska M et al (2024) New powder reuse schema in laser-based powder bed fusion of polymers. Waste Manag 187:11–21. https://doi.org/10.1016/J.WASMAN.2024.06.030
5. Kubeczek A, Olejarczyk M, Gruber P, Antończak AJ (2025) Continuous reuse of polyamide 12 in powder bed fusion. Sci Rep. https://doi.org/10.1038/s41598-025-12573-8
6. Powell D, Rennie AEW, Geekie L, Burns N (2020) Understanding powder degradation in metal additive manufacturing to allow the upcycling of recycled powders. J Clean Prod 268:122077. https://doi.org/10.1016/j.jclepro.2020.122077
7. Barclift M, Joshi S, Simpson T, Dickman C (2016) Cost modeling and depreciation for reused powder feedstocks in powder bed fusion additive manufacturing. In: Solid Freeform Fabrication 2016: Proceedings of the 27th Annual International Solid Freeform Fabrication Symposium - An Additive Manufacturing Conference, SFF 2016
8. Institute of Industrial and Systems Engineers (2018) Engineering Economic Analysis Engineering. Inst Ind Syst Eng
9. Dotchev K, Yusoff W (2009) Recycling of polyamide 12 based powders in the laser sintering process. Rapid Prototyp J. https://doi.org/10.1108/13552540910960299
10. Dadbakhsh S, Verbelen L, Verkinderen O et al (2017) Effect of PA12 powder reuse on coalescence behaviour and microstructure of SLS parts. Eur Polym J 92:250–262. https://doi.org/10.1016/j.eurpolymj.2017.05.014
11. Yang F, Schnuerch A, Chen X (2021) Quantitative influences of successive reuse on thermal decomposition, molecular evolution, and elemental composition of polyamide 12 residues in selective laser sintering. Int J Adv Manuf Technol. https://doi.org/10.1007/s00170-021-07368-w
12. Pham DT, Dotchev KD, Yusoff WAY (2008) Deterioration of polyamide powder properties in the laser sintering process. Proc Inst Mech Eng Part C J Mech Eng Sci. https://doi.org/10.1243/09544062JMES839
13. Alo OA, Otunniyi IO, Mauchline D (2023) Effects of reuse on morphology, size and shape distributions of PA 12 powder in selective laser sintering and quality of printed parts. J Polym Res. https://doi.org/10.1007/s10965-022-03423-6
14. Drummer D, Greiner S, Zhao M, Wudy K (2019) A novel approach for understanding laser sintering of polymers. Addit Manuf. https://doi.org/10.1016/j.addma.2019.03.012
15. Chen P, Tang M, Zhu W et al (2018) Systematical mechanism of Polyamide-12 aging and its micro-structural evolution during laser sintering. Polym Test. https://doi.org/10.1016/j.polymertesting.2018.03.035
16. Wudy K, Drummer D (2019) Aging effects of polyamide 12 in selective laser sintering: molecular weight distribution and thermal properties. Addit Manuf. https://doi.org/10.1016/j.addma.2018.11.007

17. Yao B, Li Z, Zhu F (2020) Effect of powder recycling on anisotropic tensile properties of selective laser sintered PA2200 polyamide. Eur Polym J. https://doi.org/10.1016/j.eurpolymj.2020.110093
18. Yang F, Zobeiry N, Mamidala R, Chen X (2023) A review of aging, degradation, and reusability of PA12 powders in selective laser sintering additive manufacturing. Mater Today Commun. https://doi.org/10.1016/j.mtcomm.2022.105279
19. Zárybnická L, Petrů J, Krpec P, Pagáč M (2022) Effect of additives and print orientation on the properties of laser sintering-printed polyamide 12 components. Polymers (Basel). https://doi.org/10.3390/polym14061172
20. Verbelen L, Dadbakhsh S, Van Den Eynde M et al (2016) Characterization of polyamide powders for determination of laser sintering processability. Eur Polym J. https://doi.org/10.1016/j.eurpolymj.2015.12.014
21. Ziółkowski G, Grochowska E, Kęszycki D et al (2021) Investigation of porosity behavior in SLS polyamide-12 samples using ex-situ X-ray computed tomography. Mater Sci Pol. https://doi.org/10.2478/msp-2021-0035
22. Lopes AC, Sampaio ÁM, Silva CS, Pontes AJ (2021) Prediction of SLS parts properties using reprocessing powder. Rapid Prototyp J. https://doi.org/10.1108/RPJ-04-2020-0076
23. Feng L, Wang Y, Wei Q (2019) PA12 powder recycled from SLS for FDM. Polymers. https://doi.org/10.3390/polym11040727
24. Kumar S, Czekanski A (2017) Development of filaments using selective laser sintering waste powder. J Clean Prod 165:1188–1196. https://doi.org/10.1016/j.jclepro.2017.07.202
25. Sanders B, Cant E, Jenkins M (2024) Re-use of polyamide-12 in powder bed fusion and its effect on process-relevant powder characteristics and final part properties. Addit Manuf. https://doi.org/10.1016/j.addma.2024.103961
26. Paolucci F, van Mook MJH, Govaert LE, Peters GWM (2019) Influence of post-condensation on the crystallization kinetics of PA12: from Virgin to reused powder. Polym (Guildf) 175:161–170. https://doi.org/10.1016/j.polymer.2019.05.009
27. Yang F, Chen X (2021) A combined theoretical and experimental approach to model polyamide 12 degradation in selective laser sintering additive manufacturing. J Manuf Process. https://doi.org/10.1016/j.jmapro.2021.08.051
28. Wörz A, Wudy K, Drummer D et al (2018) Comparison of long-term properties of laser sintered and injection molded polyamide 12 parts. J Polym Eng. https://doi.org/10.1515/polyeng-2017-0227
29. Wudy K, Drummer D (2016) Aging behavior of polyamide 12: Interrelation between bulk characteristics and part properties. In: Solid Freeform Fabrication 2016: Proceedings of the 27th Annual International Solid Freeform Fabrication Symposium - An Additive Manufacturing Conference, SFF 2016
30. Chen P, Wu H, Zhu W et al (2018) Investigation into the processability, recyclability and crystalline structure of selective laser sintered Polyamide 6 in comparison with Polyamide 12. Polym Test. https://doi.org/10.1016/j.polymertesting.2018.05.045
31. Yang F, Jiang T, Lalier G et al (2020) A process control and interlayer heating approach to reuse polyamide 12 powders and create parts with improved mechanical properties in selective laser sintering. J Manuf Process. https://doi.org/10.1016/j.jmapro.2020.07.051
32. Zhou Y, Xi S, Huang Y et al (2020) Preparation of near-spherical PA12 particles for selective laser sintering via Plateau-Rayleigh instability of molten fibers. Mater Des. https://doi.org/10.1016/j.matdes.2020.108578
33. Zarringhalam H, Hopkinson N, Kamperman NF, de Vlieger JJ (2006) Effects of processing on microstructure and properties of SLS nylon 12. Mater Sci Eng A 435–436:172–180. https://doi.org/10.1016/j.msea.2006.07.084
34. Drummer D, Rietzel D, Kühnlein F (2010) Development of a characterization approach for the sintering behavior of new thermoplastics for selective laser sintering. Phys Procedia. https://doi.org/10.1016/j.phpro.2010.08.081
35. Lammens N, Kersemans M, De Baere I, Van Paepegem W (2017) On the visco-elasto-plastic response of additively manufactured polyamide-12 (PA-12) through selective laser sintering. Polym Test. https://doi.org/10.1016/j.polymertesting.2016.11.032
36. Craft G, Nussbaum J, Crane N, Harmon JP (2018) Impact of extended sintering times on mechanical properties in PA-12 parts produced by powderbed fusion processes. Addit Manuf. https://doi.org/10.1016/j.addma.2018.06.028
37. Rouholamin D, Hopkinson N (2014) An investigation on the suitability of micro-computed tomography as a non-destructive technique to assess the morphology of laser sintered nylon 12 parts. Proc Inst Mech Eng Part B J Eng Manuf. https://doi.org/10.1177/0954405414522209
38. Calignano F, Giuffrida F, Galati M (2021) Effect of the build orientation on the mechanical performance of polymeric parts produced by multi jet fusion and selective laser sintering. J Manuf Process. https://doi.org/10.1016/j.jmapro.2021.03.018
39. Baumers M, Holweg M (2016) Cost impact of the risk of build failure in laser sintering. In: Solid Freeform Fabrication 2016: Proceedings of the 27th Annual International Solid Freeform Fabrication Symposium - An Additive Manufacturing Conference, SFF 2016
40. Sharma F, Dixit US (2019) Fuzzy set based cost model of additive manufacturing with specific example of selective laser sintering. J Mech Sci Technol. https://doi.org/10.1007/s12206-019-0840-x
41. Rickenbacher L, Spierings A, Wegener K (2013) An integrated cost-model for selective laser melting (SLM). Rapid Prototyp J 19:208–214. https://doi.org/10.1108/13552541311312201
42. Galati M, Calignano F, Viccica M, Iuliano L (2020) Additive manufacturing redesigning of metallic parts for high precision machines. Crystals. https://doi.org/10.3390/cryst10030161
43. Kopf R, Gottwald J, Jacob A et al (2018) Cost-oriented planning of equipment for selective laser melting (SLM) in production lines. CIRP Ann. https://doi.org/10.1016/j.cirp.2018.04.032
44. Ruffo M, Tuck C, Hague R (2006) Cost estimation for rapid manufacturing - Laser sintering production for low to medium volumes. Proc Inst Mech Eng Part B J Eng Manuf 220:1417–1427. https://doi.org/10.1243/09544054JEM517
45. Xue-Liang P, Chao-Lang P, Fa-Lin Z, Tong-Jun G (2007) Six Sigma approach for build-time Estimation of selective laser sintering. Int J Agil Syst Manag. https://doi.org/10.1504/ijasm.2007.015789
46. Pham DT, Wang X (2000) Prediction and reduction of build times for the selective laser sintering process. Proc Inst Mech Eng Part B J Eng Manuf. https://doi.org/10.1243/0954405001517739
47. Zhang Y, Bernard A (2014) Generic build time estimation model for parts produced by SLS. In: High Value Manufacturing: Advanced Research in Virtual and Rapid Prototyping - Proceedings of the 6th International Conference on Advanced Research and Rapid Prototyping, VR@P 2013
48. Bernardo CA (1998) Derivation and Validation of Models to Predict the Properties of Mixtures of Virgin and Recycled Polymers. Frontiers in the Science and Technology of Polymer Recycling
49. Bernardo CA, Cunha AM, Oliveira MJ (1996) The recycling of thermoplastics: prediction of the properties of mixtures of virgin and reprocessed polyolefins. Polym Eng Sci. https://doi.org/10.1002/pen.10437

50. Senthilkumaran K, Pandey PM, Rao PVM (2008) Shrinkage compensation along single direction dexel space for improving accuracy in selective laser sintering. In: 4th IEEE Conference on Automation Science and Engineering, CASE 2008
51. Senthilkumaran K, Pandey PM, Rao PVM (2009) Influence of building strategies on the accuracy of parts in selective laser sintering. Mater Des. https://doi.org/10.1016/j.matdes.2009.01.009
52. Jain PK, Pandey PM, Rao PVM (2009) Effect of delay time on part strength in selective laser sintering. Int J Adv Manuf Technol. https://doi.org/10.1007/s00170-008-1682-3
53. Singh S, Sharma VS, Sachdeva A (2012) Optimization and analysis of shrinkage in selective laser sintered polyamide parts. Mater Manuf Process. https://doi.org/10.1080/10426914.2011.593247
54. Alo OA, Otunniyi IO, Mauchline D (2023) Correlation of reuse extent with degradation degree of PA 12 powder during laser powder bed fusion and mechanical behavior of sintered parts. Polym Eng Sci. https://doi.org/10.1002/pen.26191
55. Gornet TJ, Davis KR, Starr TL, Mulloy KM (2002) Characterization of selective laser sintering materials to determine process stability. Solid Free Fabr Symp
56. Eggers T, Rackl H, von Lacroix F (2023) Investigation of the influence of the mixing process on the powder characteristics for cyclic reuse in selective laser sintering. Powders. https://doi.org/10.3390/powders2010003

Publisher's note Springer Nature remains neutral with regard to jurisdictional claims in published maps and institutional affiliations.